Available online at www.sciencedirect.com
ScienceDirect
Electrochimica Acta 53 (2007) 133–140
ELECTROCHIMICA Acta
www.elsevier.com/locate/electacta

Dense branched morphology in electrochemical deposition in a thin cell vertically oriented

G. González [a,b], A. Soba [b], G. Marshall [b,c,*], F.V. Molina [d], M. Rosso [a]

[a] *Laboratoire de Physique de la Matière Condensée, CNRS-Ecole Polytechnique, F91128 Palaiseau Cedex, France*
[b] *Laboratorio de Sistemas Complejos, Departamento de Computación, Facultad de Ciencias Exactas y Naturales, Universidad de Buenos Aires, 1428 Buenos Aires, Argentina*
[c] *Cornell Theory Center, and Laboratory for Atomic and Solid State Physics, Cornell University, Ithaca, NY 14850, USA*
[d] *INQUIMAE, Facultad de Ciencias Exactas y Naturales, Universidad de Buenos Aires, 1428 Buenos Aires, Argentina*

Received 26 November 2005; received in revised form 26 February 2007; accepted 27 February 2007
Available online 4 March 2007

Abstract

Convection due to electric and gravity forces increase complexity in thin layer electrochemistry (ECD). We describe conditions in a vertical cell with the cathode above the anode in which global convection is eliminated and a dense branched morphology with a smooth front is obtained. It is shown that these conditions allow a theoretical one dimensional modeling notably simplifying the complex analysis of the problem. We report experimental measurements under constant current conditions showing that the deposit, cathodic and proton fronts scale linearly with time, a signature of migration controlled regime. We discuss a theoretical ECD model under galvanostatic conditions with a three ion electrolyte and a growth model, consisting in the one dimensional Nernst–Planck equations for ion transport, the Poisson equation for the electric field and a growth law whose front velocity equals the anion mobility times the local electric field. The model predicts cation, anion and proton concentration profiles, electric field variations and deposit growth speed, that are in good agreement with experiments; the predicted evolution and collision of the deposit and proton fronts reveal a time scaling close to those observed in experiments.

Keywords: Electrodeposition; Thin cells; Ion transport; Numerical simulations; Migration

1. Introduction

The electrolytic cell in a thin layer cell electrodeposition (ECD) experiment, consists of a metal salt electrolyte and two parallel electrodes sandwiched within two glass plates. Fig. 1 shows such a cell in the experimental arrangement used in this work. A voltage difference applied between electrodes produces, under appropriate conditions, a ramified deposit by reduction of the metal ions. Cell geometry, its orientation relative to gravity, electrolyte concentration, cell current and other parameters, give rise to a great variety of deposit morphologies such as fractal, densely branched or dendritic. ECD is a paradigmatic model for the study of growth pattern formation, that is, the unstable growth of interfaces [1–37].

During dendrite growth, a complex ion transport process takes place, mainly governed by diffusion, migration and convection. Convection, in turn, is driven by coulombic forces due to local electric charges and by buoyancy forces due to concentration gradients that lead to density gradients. Indeed, convection increases complexity in thin layer electrochemistry. Convection can be reduced by diminishing cell thickness [24], carrying experiments in a cell with different orientations relative to gravity [23–26], increasing electrolyte viscosity [33] or under microgravity conditions [35].

In particular, in [28] were conducted ECD experiments with a cell in a vertical position. The authors found that, when the cathode (and low density fluid) is above the anode (and high density fluid), the invasion of the cell by the gravity induced rolls can be avoided while electroconvection remains. When dendrites are present, horizontal concentration gradients drive convection near the growing tips, a competition emerges in

* Corresponding author. Permanent address: Laboratorio de Sistemas Complejos, Departamento de Computación, Facultad de Ciencias Exactas y Naturales, Universidad de Buenos Aires, 1428 Buenos Aires, Argentina.
Tel.: +54 114 826 8181; fax: +54 114 576 3359.
E-mail address: marshalg@mail.retina.ar (G. Marshall).

0013-4686/$ – see front matter © 2007 Elsevier Ltd. All rights reserved.
doi:10.1016/j.electacta.2007.02.069

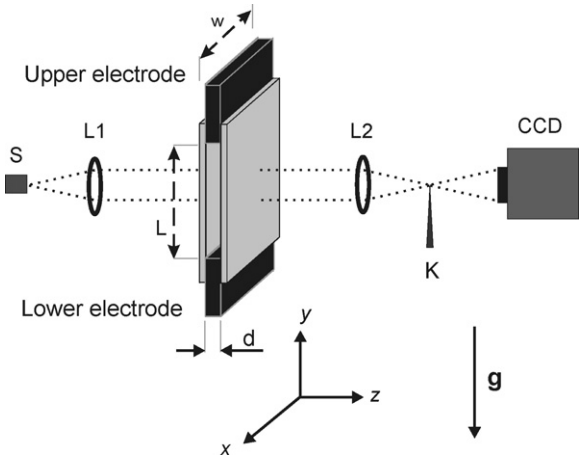

Fig. 1. Experimental setup with the cell in a vertical position with cathode as the upper electrode and anode as the lower electrode. S is a light point source. L1 and L2 are lenses. K is a knife employed for the Schlieren technique. CCD is a video camera. The coordinate system and gravity direction are shown.

which convective motion feeds branches lagging behind until they reach the leading branches. El According to the authors, this mechanism inhibits competition, leading to a uniform front rather than a hierarchy of branch sizes as seen in horizontal cells. Since convection is everywhere absent except near the growing dendrite tips, this regime is called local convection in contrast to global convection as observed in horizontal cells.

To illustrate the previous discussion, Fig. 2 shows Schlieren images (see Section 2 below) of dendrites growing from the cathode towards the anode (dark grey pixels) wrapped with concentration fronts (bright pixels). Fig. 2a corresponds to a cell in the vertical position (the plane of the growth is parallel to gravity as indicated in the figure) when the cathode is above the anode. Here, dendrites grow as a uniform front. Fig. 2b and c correspond to cells in the horizontal position (the plane of the growth is normal to gravity) in which dendrites grow as a rather uniform front (Fig. 2b) and with a hierarchy of branch sizes (Fig. 2c), respectively. While a uniform front is the exception in horizontal cells, it is the rule in vertical cells when the cathode is above the anode.

Since the pioneering work of Chazalviel [3] (see also [4]), considerable effort has been dedicated to predict ECD phenomena in cells in the horizontal position, with theoretical models and numerical simulation. In the majority of these models a binary electrolyte, fixed electrodes and potentiostatic conditions were assumed. Experimental evidence indicates that more realistic modelling should take into account proton migratory fronts [10–19,24,31], a reasonable growth law and boundary conditions for galvanostatic regimes. An effort in these directions were the works in [6], [13] and [20], where 1D and 2D ECD models, with cells in the horizontal position, with a linear growth law or with three ion electrolytes under constant voltage and steady state regimes were presented. The linear growth law was based upon the experimental evidence of several researchers showing that in many cases the deposit growth speed is equal or similar to the anion drift speed in the relatively unperturbed solution ahead of the growing tip (see for instance, [6]) and in the assumption of dense branched morphology.

In particular, a simplified 1D macroscopic model for an ECD experiment in an horizontal cell taking into account a three-ion electrolyte and a realistic aggregation model was introduced in [36]. The model revealed new insights of the fronts interaction and time scaling, but it was limited because of the need for neglecting convective effects in cells in the horizontal position. In a very recent work, [37] experimental measurements of ECD in cells in the vertical position and a 3D macroscopic model were presented. The study particularly addressed the problem of local and global convection when the cathode was above or below the anode, respectively. The model revealed useful insights but did not consider protons nor dendrite growth.

From the results presented in [37], it was possible to infer that for cells in the vertical position with the cathode above the anode, the absence of global convection and dense branched morphology, justified a simple 1D modelling. Thus, the aim of this paper is to extend the works in [24], [36] and [37], presenting new experimental measurements of ECD in cells in a vertical position with the cathode above the anode and a 1D theoretical model describing many aspects of those experiments.

The plan of the paper is the following. In Section 2, the experimental setup is presented. Section 3 describes the phenomenological model and experimental measurements. Section 4 presents a theoretical analysis and Section 5 numerical results and discussion. The last Section 6 draws some conclusions.

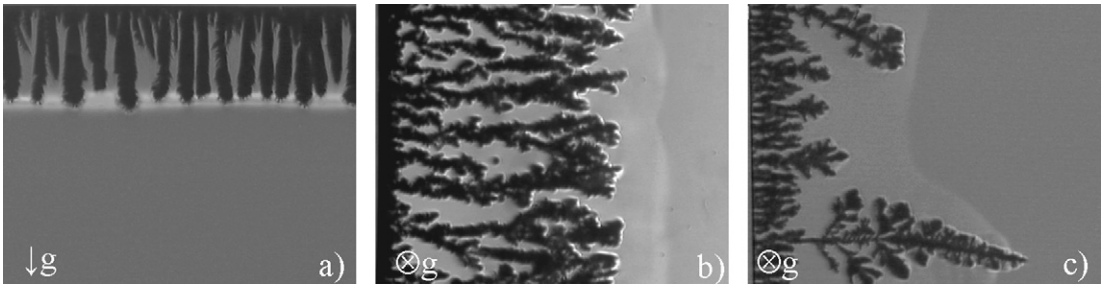

Fig. 2. Schlieren images of ECD in a cell of 10 mm × 25 mm × 0.5 mm containing $ZnSO_4$ solutions: (a) cell in the vertical position (the plane of the growth is parallel to gravity), 0.1 M, $I = 7.5$ mA, $t = 150$ s; (b) cell in the horizontal position (the plane of the growth is normal to gravity), 0.1 M with 20% glycerol added, $I = 10$ mA, $t = 220$ s and (c) cell in the horizontal position, 0.025 M, $I = 7$ mA, $t = 120$ s.

2. Experimental setup

Fig. 1 shows a typical cell in a vertical position used in ECD experiments. Here, the vertical plane or *zy* plane contains the electrodes and the growing dendrites (the cathode–anode distance is measured along the *y* axis). The cell consists of a thin layer of unsupported electrolyte confined between two parallel glass plates; cell thickness was usually 0.5, but sometimes 1.0 mm was employed to improve front observation. The electrolyte solution was 0.1–1.0 M $CuSO_4$ with the addition of 1 mM H_2SO_4 in order to have the indicator employed (see below) in its acid form initially. To increase viscosity, for some experiments, a solution with a glycerol addition of 30% in weight was employed. Both electrodes were copper plates.

The Schlieren method was used to observe electrolyte concentration gradients. The optical setup is similar to that described in [31]. Light from a bright light-emitting diode is passed through a 1 mm pinhole and collimated. After it passes through the cell, the beam is refocused by the lens L2 (Fig. 2). A knife edge K positioned parallel to the electrodes in the focal plane of L2 blocks half of the light there. The Schlieren image is viewed with a charge-coupled device (CCD) video camera with a 50 mm f/1.4 camera lens mounted beyond the knife edge. A Navitar long working distance microscope was used. Video images were digitized and saved to disk at up to 10 frames/s with a spatial resolution of up to 25 μm/pixel. A public domain software package Image [41] was used for image capturing and processing.

For studying pH fronts, light absortion techniques were used. They consist in employing the experimental setup previously described, removing the knife edge K and adding a pH indicator (Bromocresol Green, pH range 3.8–5.4) in a final concentration of 3.6×10^{-4} M. This indicator has a yellow color for pH less than 3.8 ($\lambda_{max} = 440$ nm) changing to blue ($\lambda_{max} = 615.5$ nm) at pH 5.4. The diode was chosen with a wavelength yielding maximum contrast, based upon the absortion spectra of the solution employed, with the indicator at different pH values.

3. The phenomenological model and experimental results

Here, we present a simplified version of the phenomenological model of ECD in a vertical cell with the cathode above the anode (a full description is given in [37]). When the circuit is closed, the copper metal anode dissolves yielding Cu^{2+} ions and at the cathode the opposite reaction takes place. In the relatively concentrated solutions employed, transition metal ions such as Cu^{2+} undergo hydrolysis reactions:

$$Cu(H_2O)_6{}^{2+} \rightarrow Cu(H_2O)_5OH^+ + H^+ \quad (1)$$

As it is well known, transition metal solutions have an acidic pH. In the case of $CuSO_4$, a 0.1 M solution should have a pH of about 4.5 (calculated using an speciation program such as Visual minteq [42]). When concentration increases at the anode due to metal dissolution and anion accumulation, the H^+ concentration should increase, producing a proton migration wave, termed pH front, which causes the Hecker effect [10].

Assuming, as previously discussed, that ion transport is solely governed by diffusion and migration and a dense branched morphology, when the circuit is closed, two concentration fronts emerge from each electrode advancing in opposite directions.

Concomitantly, the deposit front advances towards the anode with a velocity proportional to the anion mobility times the electric field and a pH front emanating from the anode moves towards the cathode with a velocity proportional to the proton mobility times the electric

The point of intersection between the pH and the deposit fronts reveals the Hecker effect [10] that induces a change in the deposit growth rate (associated with a morphology change). The figure also reveals the second transition in the deposit growth rate when the deposit meets the anodic concentration front. At the bottom of Fig. 3, a snapshot at 160 s of a top view of a portion of the cell is presented.

Comparing Fig. 3 with a similar figure obtained in [24] (Fig. 9) for a cell in an horizontal position, we note the differences: the absence of global convection due to buoyancy effects (absence of gravitoconvective rolls) and a retardation in fronts speeds in the case of the vertical cell.

Fig. 4 shows absortion intensity measurements of deposit and pH concentration fronts as a function of position in the cell, for different times (before and after the onset of growth). The pixel intensity changes sharply in small regions close to the deposit front; the position of these changes are taken as the locations of the deposit front.

Figs. 5 and 6 show the time evolution of the pH and deposit fronts, respectively, for different applied electric currents (2.5, 5.0, 7.5 y 10 mA), in a 0.5 mm thickness cell. Both fronts scale linearly with time showing a migration controlled ion transport.

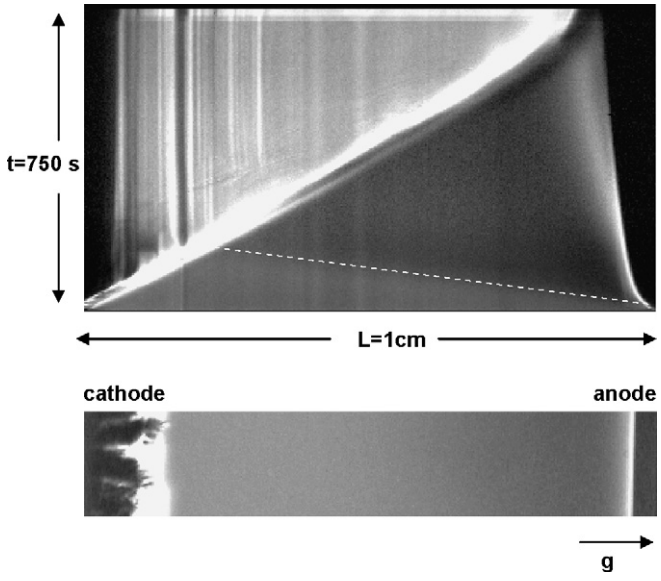

Fig. 3. Space time evolution of the ion transport modes in a vertical cell. The top figure shows the deposit front (dark pixels with vertical strips at the left), wrapped with the cathodic concentration front (bright pixels), the pH front (light grey pixels at the bottom where the dotted line emphasize the border of the pH front) and the anodic concentration front (dark pixels at the far right). The bottom picture shows a snapshot of the cell (dendrites and concentration fronts) at 160 s. This experiment was conducted in a cell with $d = 1.00$ mm under $I = 10$mA.

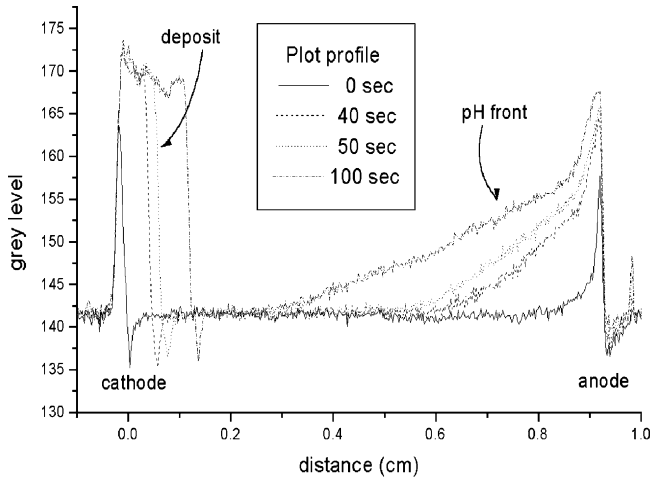

Fig. 4. Schlieren pixel intensity of deposit and pH concentration fronts as a function of position in the cell, for different times (before and after the onset of growth). Images at 0, 40, 50 and 100 s with 10 mA, in a 0.5 mm thickness cell.

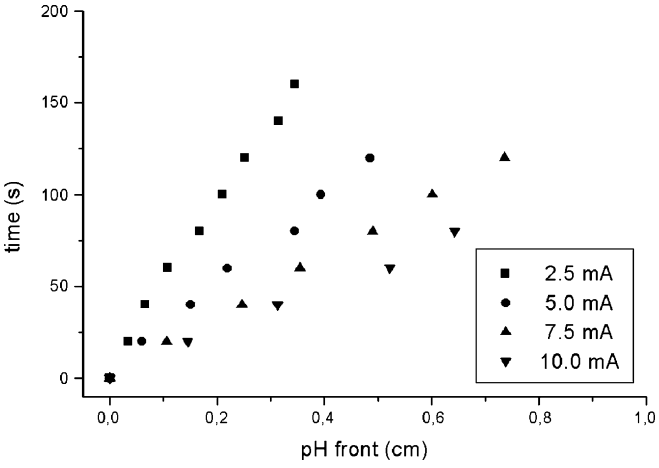

Fig. 5. pH space time evolution for 2.5, 5.0, 7.7 and 10 mA.

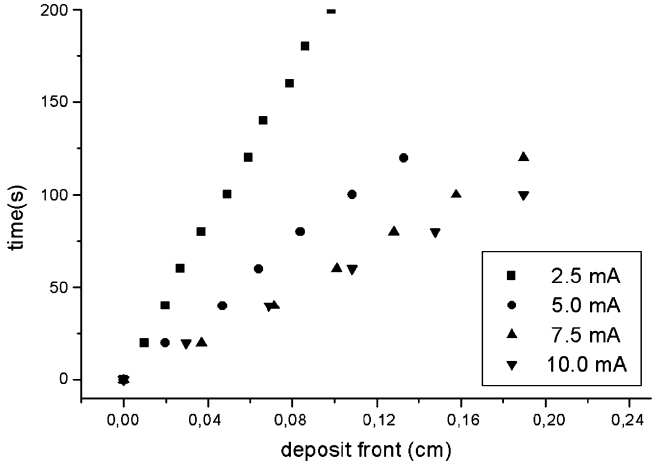

Fig. 6. Deposit front space time evolution for 2.5, 5.0, 7.7 and 10 mA.

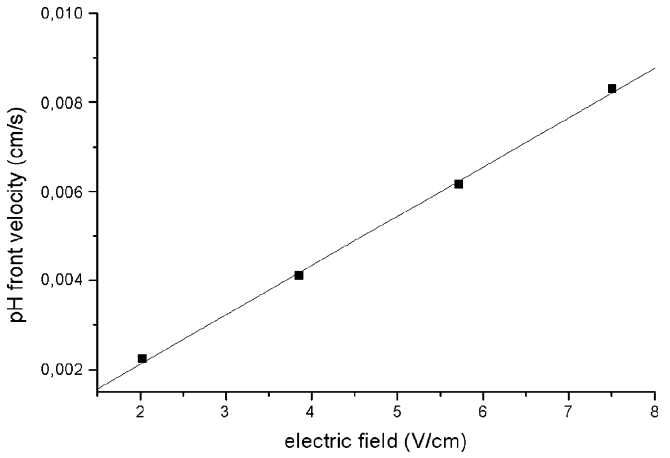

Fig. 7. pH front slope as a function of the initial electric field. The straight line is a linear fit.

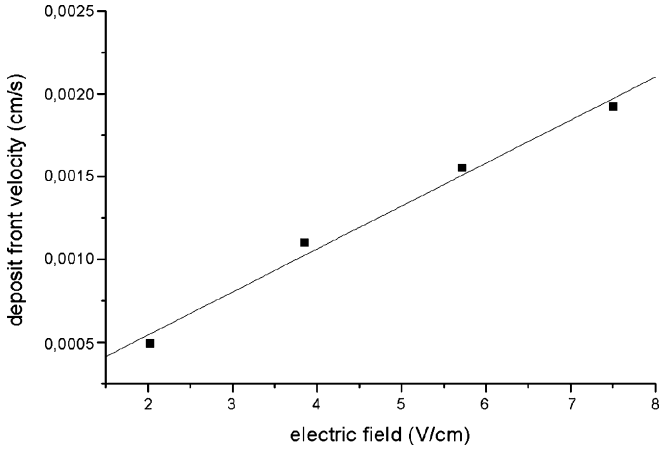

Fig. 8. Deposit front slope as a function of the initial electric field and its linear fit.

Figs. 7 and 8 show the corresponding pH and deposit fronts slopes as a function of the initial electric field and a straight linear fit superimposed.

Assuming that the deposit front velocity is given by $\mathbf{v} = \mu_A \mathbf{E}$, where $\mathbf{v}$ is the deposit front velocity, $\boldsymbol{\mu}_a$ is the anion mobility and $\mathbf{E}$ the electric field, from the straight lines from Figs. 7 and 8 we obtain: $\mu_H = 1.1 \times 10^{-3}\ \mathrm{cm^2\ V^{-1}\ s^{-1}}$, and $\mu_{SO_4} = 2.6 \times 10^{-4}\ \mathrm{cm^2\ V^{-1}\ s^{-1}}$. These magnitudes are slightly smaller than infinite dilution mobilities ($\mu_H = 3.6 \times 10^{-3}\ \mathrm{cm^2\ V^{-1}\ s^{-1}}$ and $\mu_{SO_4} = 8.5 \times 10^{-4}\ \mathrm{cm^2\ V^{-1}\ s^{-1}}$), as expected. We note that in experiments without pH indicator, we obtained a value of $\mu_{SO_4} = 2.8 \times 10^{-4}\ \mathrm{cm^2\ V^{-1}\ s^{-1}}$, thus showing that there is no significant difference with or without pH indicator for deposit front evolution.

4. Theoretical analysis

In Section 3, we presented a phenomenological 1D macroscopic ECD model for a three ion electrolyte with a cell in the vertical position and the cathode above the anode. It was shown there that global convection was totally suppressed. Accordingly, the phenomenological model can be described in one

dimension using the Nernst–Planck equations for ion transport [38–40] and the Poisson equation for the electric potential. This is combined with an aggregation model describing the advance of the deposit. Here, we assume, following [6] that the deposit front advances with velocity equal to the anion mobility times the electric field, which is consistent with a densely branched morphology. Morphology transitions can only occur when incoming fronts collide with the deposit front: in the present model, their space location can be predicted, tracking ion concentration fronts and their collision with the deposit front. This is allowed because of the absence of global convection. The one dimensional system of equations in dimensionless form can be written as (see Fig. 1 for the reference frame)

$$\frac{\partial C_i}{\partial t} = -\nabla \cdot \mathbf{j}_i \tag{2}$$

$$j_i = -M_i C_i \nabla\phi - \frac{1}{Pe_i}\nabla C_i \tag{3}$$

$$\nabla^2\phi = Po\sum_i z_i C_i \tag{4}$$

Here, ϕ is the dimensionless electrostatic potential, C_i and $\mathbf{j}_i$ are the dimensionless concentration and flux of the ionic species i, where $i = C$, A and H, standing for Cu^{2+}, $SO_4{}^{2-}$ and H^+ ions, respectively. Hydrogen ions are present due to either H_2SO_4 addition or to the hydrolysis of the salt cation (Eq. (1)); as said previously, acid is added in order to bring the indicator fully to its acid form. The $CuOH^+$ ions produced in the hydrolysis having a lower concentration (about 2×10^{-5} M in a 0.1 M $CuSO_4$ solution) and roughly half the mobility than Cu^{2+}, will be neglected.

The quantities $M_i = \mu_i\phi_0/x_0u_0$, $Pe_i = x_0u_0/D_i$, and $Po = x_0{}^2C_0e/\varepsilon\phi_0$, stand for the dimensionless numbers Migration, Peclet, and Electric Poisson, respectively (see details in [37]). The quantities z_i, μ_i, and D_i are respectively the charge number, mobility and diffusion coefficient of an ionic species i; μ_i and z_i are signed quantities, being positive for cations and negative for anions; e is the electronic charge, and ε is the permittivity of the medium. x_0, u_0, ϕ_0, and C_0, are reference values of the length, velocity, electrostatic potential, and concentration, respectively (later discussed).

Under a constant current ECD simulation, the boundary conditions for the cathode and the deposit ($y = y_0$, where y_0 is the deposit front position; in the absence of deposit $y_0 = 0$), following [36] are:

$$\phi(y_0) = \frac{kT}{ze\phi_0}\ln(C_C(y_0, t)) \tag{5}$$

$$\left.\frac{\partial C_C}{\partial y}\right|_{y_0} = 0 \tag{6}$$

$$\left.\frac{\partial C_H}{\partial y}\right|_{y_0} = 0 \tag{7}$$

$$j_A(y_0) = 0 \tag{8}$$

where j_C is the cation flux, and J is the current density. The boundary conditions for the anode ($y = 1$) are:

$$\phi(1) = J\int_0^1 \frac{dy}{\sum_i z_i C_i \mu_i} \tag{9}$$

$$j_C(1) = \frac{\theta J}{z_C e} \tag{10}$$

$$j_H(1) = \frac{(1-\theta)J}{z_H e} \tag{11}$$

$$j_A(1) = 0 \tag{12}$$

where θ is a parameter varying between 0 and 1, its meaning later explained, and in Eq. (8), the cell resistivity is assumed to be of migratory nature, thus neglecting diffusion effects in calculating the total voltage drop in the cell.

As discussed in Section 1, the high concentration of metal cations generated by anode dissolution causes a local acidification due to a reaction described in Eq. (1), which is expected to be much faster than the transport processes. From the equilibrium constant and appropriate activity coefficients, the local H^+ concentration could be computed. However, as discussed below, due to numerical constraints we are forced to use values for the dimensionless numbers which correspond to concentrations considerably lower than typical experimental values. Because of this, and also because we are mainly interested in the study of front evolution, a parameter θ is introduced in Eqs. (9) and (10) to simulate the presence of protons in the vicinity of the anode. θ is taken as the fraction of the anodic charge effectively resulting in the introduction of metal cations (θ represents the fraction of current spent in generating metal cations). Thus, $\theta = 1$ means that only Cu^{2+} cations are produced (so that no anodic proton wave will be present), whereas $\theta = 0$, corresponds to the (hypothetical) case where only H^+ ions appear at the anode. For convenience, a second parameter θ_0 representing the initial cation concentration in the cell is introduced. Clearly, θ_0 is used to specify the initial $CuSO_4/H_2SO_4$ ratio: θ_0 is the fraction of $CuSO_4$ and $(1–\theta_0)$ is the fraction of H_2SO_4. Thus, at $t = 0$, the dimensionless anion concentration C_A is uniform and equal to 1, the Cu^{2+} concentration C_C is equal to θ_0 and the H^+ concentration C_H equals $2(1–\theta_0)$. Also, at $t = 0$ the electrostatic potential is a ramp function between the cathode ($\varphi = 0$) and the anode ($\varphi = 1$).

Typical experimental values of the dimensionless numbers in a cell with $L = 1.5$ cm, $d = 0.05$ cm, $C = 0.1$ M and $I = 10$ mA, result in: $M_C = 0.66$, $M_A = 1.0$, $M_H = 4.4$, $Pe_C = 18$, $Pe_A = 12$, $Pe_H = 2.7$, $Po = 18 \times 10^8$ (the reference values used here were: $x_0 = d$ and $u_0 = \mu_A E_0 = \mu_A\phi_0/x_0$ [35]). The range of values of the dimensionless numbers reflects the disparity of scales of the processes involved in ECD [37] yielding a stiff numerical problem.

The one dimensional system is solved, for each time step in a moving domain on a two dimensional uniform lattice using finite differences and deterministic relaxation techniques, under galvanostatic conditions. As shown in [36], in the case of a moving cathode, in each time step, given the voltage V at the bound-

aries, ion concentrations and the potential are calculated inside the cell; the front is then advanced with a velocity proportional to the anion mobility times the electric field. For advancing the front, in [36], an empirical functional relation between the front velocity and the electric field is imposed, in which the mobility is considered constant and the electric field is calculated at each time step, as the average of the local electric field in front of the deposit. This value emerges, at each time step, from the numerical solution of the complete system of equations. In the simulation of a galvanostatic experiment, in each time step, given the electric current density J, the global voltage drop is computed through Ohm's law using the migratory cell resistance Eq. (8). The calculated voltage is used as a boundary condition and the calculation proceeds as in the potentiostatic case (see [36] for details), except for the remaining boundary conditions that now must satisfy Eqs. (5)–(12).

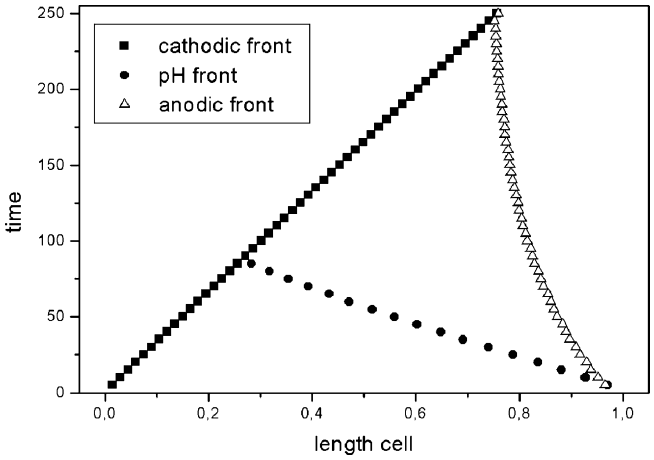

Fig. 9. Full space time evolution simulation of the ion transport modes in a vertical cell: deposit and cathodic concentration fronts coinciding, both emerging from the left, the pH front (straight line) and the anodic concentration front (curved) emerging from the right ($I = 10$ mA).

5. Numerical results and discussion

Here, we present numerical simulations with the aim of describing ECD experiments in a vertical cell. The ECD experiments from Fig. 3 are mimicked with a ternary electrolyte and moving boundaries (dense branched morphology assumption) under galvanostatic conditions. The disparity of scales of the processes being simulated precludes the use of some of the real dimensionless numbers; in particular, the value of the Poisson number employed in the simulations ($Po = 50$) differ considerably from those found in typical experiments. The computational model is written in the C language and implemented on a Pentium class computer. All the results are plotted in dimensionless form. The initial and boundary conditions for the protons are mimicked with the values $\theta_0 = 0.99$ (proton production at the anode is considered negligible in comparison with the acid already present), and the deposit front is advanced proportional to the electric field times the anion mobility.

Fig. 9 shows simulated deposit and pH front trajectories under galvanostatic conditions (the characterization of the proton trajectory has been obtained numerically as follows: a time stack formed with the successive values of the proton concentration for different time steps results in a space time surface $C_H(y, t)$, a particular contour of which is plotted in the figure).

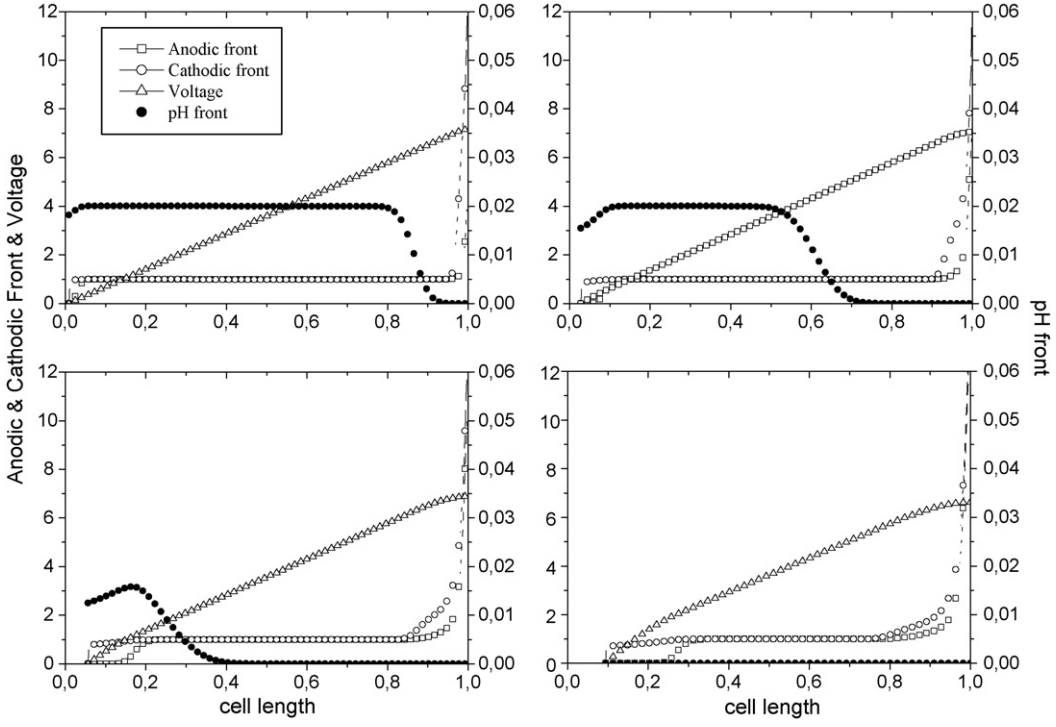

Fig. 10. Simulated cationic and anionic concentrations, pH fronts and potential, at different times in lexicographic ordering ($t = 10$, 30, 60 and 100, $I = 10$ mA).

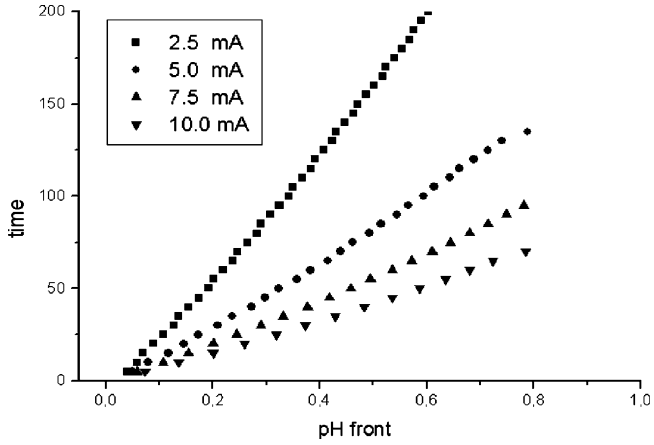

Fig. 11. Simulated pH front space time evolution for 2.5, 5.0, 7.5 and 10 mA.

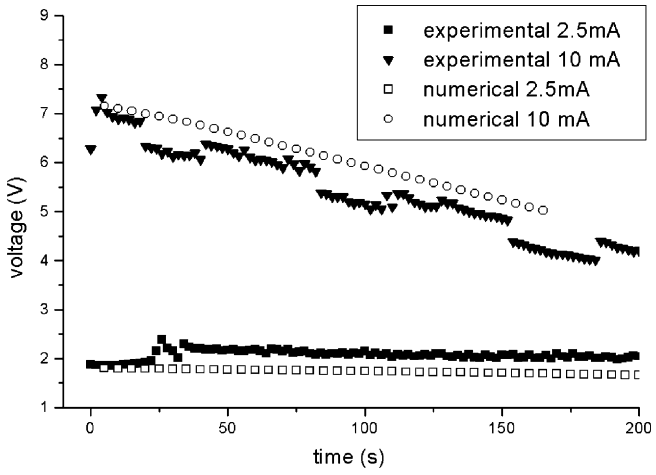

Fig. 13. Experimental and simulated voltages at constant I (2.5 and 10 mA).

As observed in the figure, the deposit front reaches the proton depletion front at about $t = 80$ at a position $y \approx 0.3$, in reasonable agreement with the experimental results of Fig. 5 ($y \approx 0.35$). In our model, no change in the velocity of the front is observed in its encounter with the protonic front.

The deposit front speed is simulated as the experimental measure of the anion mobility times the average electric field in front of the deposit. The use of an averaged field approximation to simulate the deposit front speed appears to be reasonable, since this trajectory limits the evolution of a depletion zone with a high potential drop concentrated in a small spatial range.

Fig. 10 shows the potential and concentration profiles at different times predicted by our 1D model. Initially, there is a uniform ion concentration (cations and ions). As time evolves, two concentration fronts emerge from each electrode advancing in opposite directions, a deposit front advances towards the anode with a velocity proportional to the anion mobility times the electric field, and a high pH front (that is, a depletion of H^+ ions) emanating from the anode moves towards the cathode with a speed of a migration front. Cation and anion concentrations are in qualitative agreement with the experimental profiles of Fig. 4.

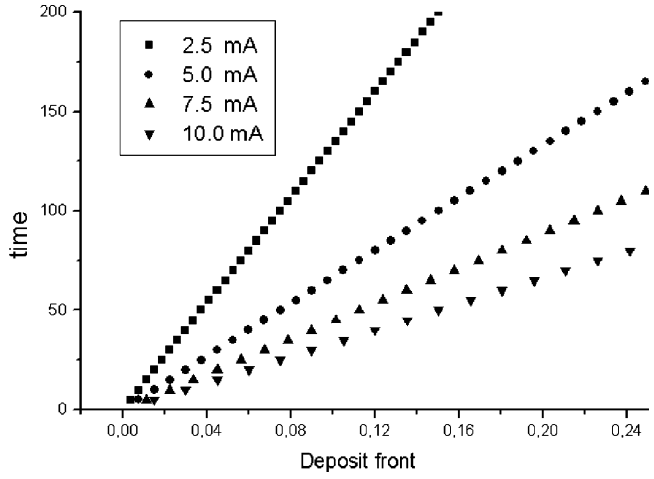

Fig. 12. Simulated deposit front space time evolution for 2.5, 5.0, 7.5 and 10 mA.

Figs. 11 and 12 show the time evolution of the simulated pH and deposit fronts, respectively, for different applied electric currents ($I = 2.5$, 5.0, 7.5 and 10 mA). As seen in the figures, both fronts scale linearly with time showing a migration controlled ion transport, in excellent agreement with the experimental evidence shown in Figs. 5 and 6.

Fig. 13 shows the time evolution of simulated and experimental voltages for constant currents (2.5 and 10 mA). These results demonstrate that, although being a crude one-dimensional approximation, the theoretical model presented here captures the essence of the ECD.

6. Conclusions

We described conditions in a vertical cell with the cathode above the anode in which global convection is eliminated and a dense branched morphology with a smooth front is obtained. It is shown that these conditions allow a simplified theoretical modeling notably simplifying the complex analysis of the problem. We reported experimental measurements for ECD in a cell in the vertical position with the cathode above the anode and in the presence of dense branched morphology showing that the pH and deposit fronts are migratory controlled. We discussed a 1D theoretical model describing a three ion transport with an aggregation model. The theoretical model predicts, ionic concentration profiles, electric field variations and deposit growth speed that are in good agreement with experiments; moreover, the evolution and collision of the deposit and proton fronts reveal a time scaling close to those observed in experiments.

Acknowledgements

G.G., G.M. and F.V.M. are investigators at the National Research Council of Argentina (CONICET). A.S. is partially supported by University of Buenos Aires (UBA). This work was partially supported by grants from UBACyT X122/04, ANPCyT: PICTR 184, CONICET: PIP 379/98 and Microsoft RFP2006 Digital Inclusion in Health and Higher Education.

References

[1] T. Vicsek, Fractal Growth Phenomena, second ed., World Scientific, Singapore, 1992.
[2] F. Argoul, J. Huth, P. Merzeau, A. Arneodo, H.L. Swinney, Physica D 62 (1993) 170.
[3] J.N. Chazalviel, Phys. Rev. A 42 (1990) 7355.
[4] J.N. Chazalviel, Coulomb Screening by Mobile Charges Applications to Material Science, Chemistry, and Biology, Birkhauser Verlag, 1999.
[5] R.M. Brady, Ball, Nature (Lond.) 309 (1984) 225.
[6] V. Fleury, J.N. Chazalviel, M. Rosso, B. Sapoval, Phys. Rev. A 44 (1991) 6693.
[7] V. Fleury, J.N. Chazalviel, M. Rosso, Phys. Rev. Lett. 68 (1992) 2492.
[8] V. Fleury, J.N. Chazalviel, M. Rosso, Phys. Rev. E 48 (1993) 1279.
[9] D. Barkey, P. Garik, E. Ben-Jacob, B. Millar, B. Orr, J. Electrochem. Soc. 139 (1992) 1044.
[10] N. Hecker, D.J. Grier, L.M. sander, in: R.B. Leibowitz, B.B. Mandelbrot, D.E. Passoja (Eds.), Fractal Aspects of Materials, Materials Research Society, University Park, PA, 1985.
[11] P. Garik, D. Barkey, E. Ben-Jacob, E. Bochner, N. Broxholm, B. Miller, B. Orr, R. Zamir, Phys. Rev. Lett. 62 (1989) 2703.
[12] J.R. Melrose, D.B. Hibbert, R.C. Ball, Phys. Rev. Lett. 65 (1990) 3009.
[13] V. Fleury, M. Rosso, J.N. Chazalviel, Phys. Rev. A 43 (1991) 6908.
[14] P. Trigueros, J. Claret, F. Mas, F. Sagues, J. Electroanal. Chem. 312 (1991) 219.
[15] A. Kuhn, F. Argoul, Fractals 1 (1993) 451.
[16] P. Carro, S.L. Marchiano, A. Hernandez Creus, S. Gonzalez, R.C. Salvarezza, A.J. Arvia, Phys. Rev. E 48 (1993) 2374.
[17] A. Kuhn, F. Argoul, J. Electroanal. Chem. 371 (1994) 93.
[18] A. Kuhn, F. Argoul, Phys. Rev. E 49 (1994) 4298.
[19] D. Otero, G. Marshall, S. Tagtachian, Fractals 4 (1996) 7.
[20] P.P. Trigueros, F. Sagues, J. Claret, Phys. Rev. E 49 (1994) 4328.
[21] V. Fleury, J. Kaufman, B. Hibbert, Nature 367 (1994) 435.
[22] K.A. Linehan, J.R. de Bruyn, Can. J. Phys. 73 (1995) 177.
[23] M. Rosso, J.N. Chazalviel, V. Fleury, E. Chassaing, Electrochem. Acta 39 (1994) 4.
[24] J. Huth, H. Swinney, W. McCormick, A. Kuhn, F. Argoul, Phys. Rev. E 51 (1995) 3444.
[25] J.R. de Bruyn, Phys. Rev. Lett. 74 (1995) 4843.
[26] M.Q. Lopez-Salvans, P.P. Trigueros, S. Vallmitjana, J. Claret, F. Sagues, Phys. Rev. Lett. 76 (1996) 4062.
[27] D. Barkey, in: Alkire, Kolb (Eds.), Structure and Pattern Formation in Electrodeposition, Advances in Electrochemical Science and Engineering, vol. 7, Wiley-VCH, 2000.
[28] G. Marshall, E. Perone, P. Tarela, P. Mocskos, Chaos, Solitons Fractals 6 (1995) 315.
[29] G. Marshall, P. Mocskos, Phys. Rev. E 55 (1997) 549.
[30] G. Marshall, P. Mocskos, H.L. Swinney, J.M. Huth, Phys. Rev. E 59 (1999) 2157.
[31] S. Dengra, G. Marshall, F. Molina, J. Phys. Soc. Jpn. 69 (2000) 963.
[32] G. Gonzalez, G. Marshall, F.V. Molina, S. Dengra, M. Rosso, J. Electrochem. Soc. 148 (2001) C479.
[33] G. Gonzalez, G. Marshall, F.V. Molina, S. Dengra, Phys. Rev. E 65 (2002) 051607.
[34] G. Marshall, E. Mocskos, F.V. Molina, S. Dengra, Phys. Rev. E 68 (2003) 021607.
[35] Y. Fukunaka, K. Okano, Y. Tomii, Z. Azaki, J. Electrochem. Soc. 145 (6) (1998) 1876.
[36] G. Marshall, F.V. Molina, A. Soba, Electrochem. Acta 50 (2005) 3436.
[37] G. Marshall, E. Mocskos, G.A. Gonzalez, S. Dengra, F.V. Molina, C. Iemmi, Electrochem. Acta 51 (2006) 3058.
[38] A.J. Bard, L.R. Faulkner, Electrochemical Methods, Fundamentals and Applications, Wiley, New York, 1980.
[39] J.S. Newman, Electrochemical Systems, Prentice Hall, New Jersey, 1973.
[40] R.F. Probstein, Physicochemical Hydrodynamics, An Introduction, Wiley, New York, 1994.
[41] Nih Image, an image processing and analysis package, free downloaded at http://rsb.info.nih.gov/nih-image/index.html.
[42] Visual minteq (Vminteq), a chemical speciation program, free downloaded at http://www.lwr.kth.se/English/OurSoftware/vminteq/.